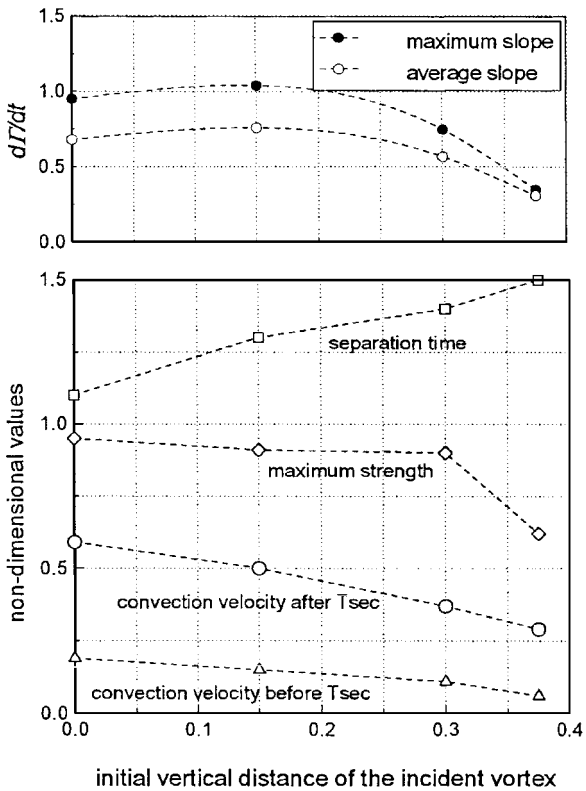

Fig. 4 Behavior of the secondary vortex. T_{sec} is the separation time when the secondary vortex departs the edge of the wedge.

the behaviors of the secondary vortex are summarized as follows: The convection velocities decrease linearly, and the separation time retards linearly, whereas the maximum strengths are almost constant between $0.0 \sim 0.3$ of y_v.

One of the important parameters related to the unsteady force variation is the time rate change of vortex strength, i.e., $d\Gamma/dt$, where Γ is the strength of the secondary vortex. The peak and the average values of $d\Gamma/dt$ to y_v are also plotted in Fig. 4, where the average value is a mean slope from the value at time $= 0.5$ to the maximum value of the strength. The values of $d\Gamma/dt$ are largest at $y_v = 0.15$ in both calculations, which indicates that the secondary vortex is formed quickly in that case because of a relatively greater dive effect[2] of the larger portion of the incident vortex, so that the pressure or unsteady force variation will be great for the case.

III. Conclusion

Numerical simulation of a single vortex-wedge interaction is conducted by using a fast vortex method that combines the Lagrangian random vortex method with the Eulerian method to include viscous and inviscid effects, respectively. The time variation of the strength of the secondary vortex and its convection velocity are calculated for several values of the initial vertical distance between the incident vortex and the wedge. Within the distance of the incident vortex diameter, the maximum strengths of the secondary vortex are almost constant, and the convection velocities show linear trends with the vertical distance changes. However, the time rate change of the strength of the secondary vortex has the largest value for the $y_v = 0.15$, just above the center line, indicating a relatively quick formation of the secondary vortex and a large contribution to the force on the wedge.

References

[1]Rockwell, D., "Oscillations of Impinging Shear Layers," *AIAA Journal*, Vol. 21, No. 5, 1983, pp. 645–664.

[2]Ziada, S., and Rockwell, D., "Vortex-Leading Edge Interaction," *Journal of Fluid Mechanics*, Vol. 118, 1982, pp. 79–107.

[3]Park, J. H., and Lee, D. J., "Numerical Simulation of Vortex-Wedge Interaction," *AIAA Journal*, Vol. 32, No. 6, 1994, pp. 1126–1134.

[4]Barker, S. J., and Crow, S. C., "The Motion of Two-Dimensional Vortex Pairs in a Ground Effect," *Journal of Fluid Mechanics*, Vol. 82, Pt. 4, 1977, pp. 659–671.

[5]Shih, C., Lourenco, L., Van Dommelen, L., and Krothapalli, A., "Unsteady Flow Past an Airfoil Pitching at a Constant Rate," *AIAA Journal*, Vol. 30, No. 5, 1992, pp. 1153–1161.

S. Glegg
Associate Editor

Laser-Induced Spark Schlieren Imaging

B. Zakharin,* J. Stricker,† and G. Toker‡
Technion—Israel Institute of Technology, 32000 Haifa, Israel

Introduction

THE transmission of light beams through compressible turbulent flowfields, with index-of-refraction variations, has recently been extensively studied.[1,2] The main interest in these studies is to evaluate the optical characteristics of airborne imaging, tracking, and irradiating systems. The analysis of the aberrated beams can be accomplished with optical diagnostic techniques such as schlieren, moire, Hartmann sensor, interferometry, holography, etc.[2,3]

Most of the experimental work published on this subject had been performed with the diagnostic light beam being transmitted through the flowfield in a direction perpendicular to the flow axis. The drawback of these measurements is that the measured light beam degradation is also caused by, in addition to the flowfield around the model, the wind-tunnel walls' boundary layers through which the beam is transmitted. These undesired effects cannot easily be separated from the pure effect of the flowfield disturbance caused by the model itself.[4,5] Measuring the aberrations directly in the streamwise direction is very complicated because it is impossible to insert a light source into the system without disturbing the flow. Transmitting the light beam through the end wall of the system along the flow axis does not solve the problem, as the beam suffers aberrations while propagating through various optically unclean regions such as nozzle flow, rarefaction, and pressure waves. The focusing schlieren method[6,7] overcomes this problem only to a certain degree because the method does not compensate for optical flaws of all dimensions.

It is our objective in this Note to propose a schlieren system in which the light source is inserted into the flow upstream of the model without disturbing the flow. The concept of such a system is shown in Fig. 1. The light source suggested is a spark generated by electrical breakdown of the air, in focal point SP of a focused high-power infrared pulsed laser. In this case, focusing lens L_1 is positioned on the model itself. The beam is transmitted through the two antireflection-coated windows, W_1 and W_2, and reflected from mirror M before arriving at L_1. Mirror M is transparent to the visible light.

When the power in the focal region reaches a critical threshold value, electrical breakdown of the gas will occur and the associated plasma appears as a very luminous bluish-white spark. An excellent summary of the breakdown and spark phenomena is contained in the book by Hughes.[8] Lens L_1 collimates the light emitted from the spark, which is automatically located at its focal distance from the spark. Lens L_2 at its focal plane forms the image of the spark where knife edge KE is located. Lens L_3 serves to image the phase object on the photographic film or charge-coupled-device camera, thereby eliminating possible shadowing effects.

Received 14 September 1998; revision received 8 March 1999; accepted for publication 13 March 1999. Copyright © 1999 by the American Institute of Aeronautics and Astronautics, Inc. All rights reserved.

*Graduate Student, Faculty of Aerospace Engineering.
†Associate Professor, Faculty of Aerospace Engineering. Member AIAA.
‡Research Engineer, Faculty of Aerospace Engineering.

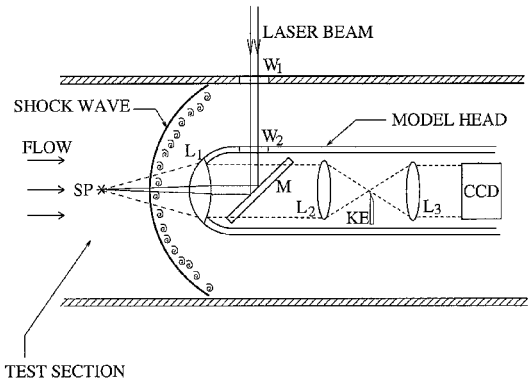

Fig. 1 Schlieren system with a laser-induced spark.

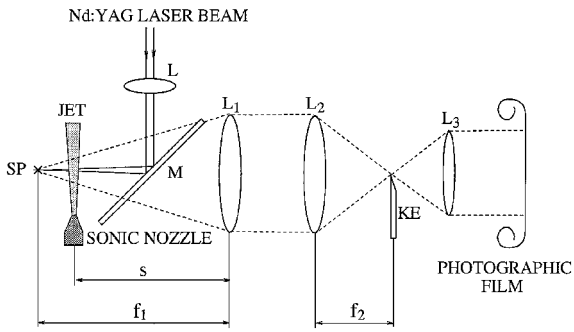

Fig. 2 Experimental setup for small sonic free jet schlieren imaging.

The proposed method can be used as well in other experimental systems in which inserting a source point can be of great value. These include cases in which there is limited optical access or in which the viewing angle desired prevents conventional imaging systems from being effectively used.

Another interesting schlieren system with an external light source has been suggested by Weinstein et al.[9] They developed a schlieren imaging system that uses the sun as a light source to obtain flowfield images of aircraft in flight.

In the following section a demonstration of the schlieren system is described.

Experimental

The method has been demonstrated by the imaging of a small, 2-mm-diam sonic jet. The experimental system is shown in Fig. 2. A pulsed Q-switched Nd:YAG laser has been used. The laser radiates at 1.064 μm with an energy of 300 mJ per pulse and a duration of 10 ns. The spark produced has a cylindrical–conical shape with a diameter of $\sim$2 mm and a duration of $\sim$0.2 μs.

From Fig. 2 it is seen that in the present system the phase object is placed in the diverging beam at a distance s from L_1, rather than in the parallel beam region, as in conventional schlieren systems.[3,10] The use of the diverging geometry is a little inconvenient for quantitative investigation since the shift δ of the light source image (in the knife-edge plane) is dependent on the distance s.

For the paraxial approximation, the displacement of the spark image δ, because of the angular deflection of the optical rays ε caused by the phase object, is given by

$$\delta = (f_1 - s)(f_2/f_1)\varepsilon$$

This equation reveals that the sensitivity of the system increases when the distance s is shortened and the ratio f_2/f_1 is increased.

A typical schlieren photograph of the free jet is shown in Fig. 3a. For comparison, a schlieren photograph without the jet is shown in Fig. 3b. From Fig. 3a it can be seen that the system is of high spatial resolution. Turbulent density structures of the order of 0.1 mm are clearly resolved. Schlieren images of steady objects taken with consequent laser pulses were highly reproducible.

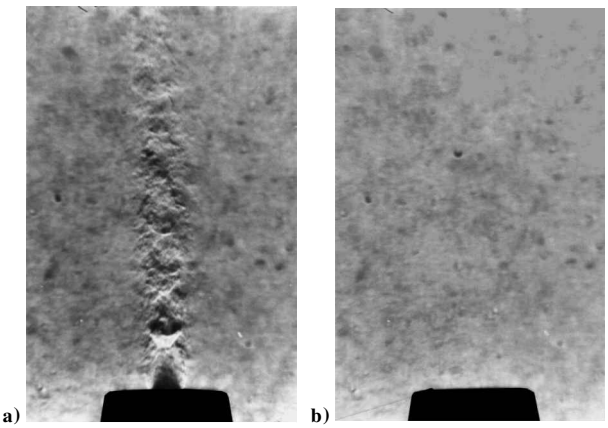

Fig. 3 Schlieren photographs taken with the system shown in Fig. 2 a) with the presence of the jet and b) without the jet. Size of the jet at the exit, ~ 2 mm.

The blurred low-contrast structure superimposed on the turbulent jet schlierengraph is due to the low quality of mirror M. The same structure appears in Fig. 3b. In principle, one can get rid of this structure by subtracting the pattern of Fig. 3b from that of Fig. 3a.

Note that Figs. 3a and 3b do not show any traces of the blast wave accompanying the electrical breakdown. This fact is expected because the luminous spark is over when the blast wave emanates out of the spark boundaries.

Other noncoherent optical techniques, such as moire deflectometry[11] or a Hartmann sensor, can also be used with the spark source system.

Two additional important remarks have to be made:

1) As mentioned earlier, the spark has a cylindrical–conical shape, with the axis along the focusing beam. It has been noted that the sparks generated by successive laser pulses were not located exactly at the same fixed position, but rather fluctuate a little along the direction of the beam axis. Apparently the arrangements shown in Figs. 1 and 2 are not sensitive either to the cylindrical shape or to the small fluctuations of the spark. However, when focusing is along a direction perpendicular to the schlieren system axis, the fluctuations of spark location will cause the spark image to move in a perpendicular direction relative to the knife edge and thus change the alignment of the system. For this case, the cylindrical shape of the spark may reduce the system sensitivity.

2) The laser beam propagates through various optically disturbed regions before arriving at focal point SP. The effect of these disturbances is mainly to increase the threshold energy of the laser required for breaking down the air.

Conclusion

It has been shown that a laser-induced spark is suitable for serving as the light source in a schlieren system, in which it is impossible to install a conventional light source in the test section. The schlieren system is of short duration, enabling us to photograph instantaneous density fields. The system is reproducible with high resolution. Optical aberrations, caused by flaws in the optical components, may be subtracted.

Acknowledgment

The authors are grateful to Samuel Mangoubi for stimulating interest in the subject.

References

[1]Sutton, G. W., "Aero-Optical Foundations and Applications," *AIAA Journal*, Vol. 23, No. 10, 1985, pp. 1525–1537.

[2]Jumper, E. J., "Recent Advances in the Measurement and Analysis of Dynamic Aero-Optic Interaction (Review Paper)," AIAA Paper 97-2350, June 1997.

[3]Merzkirch, W., *Flow Visualization*, Academic, New York, 1987.

[4]Havener, G., and Kirby, D., "Aero-Optical Phase Measurements Using Fourier Transform Holographic Interferometry," *AIAA Journal*, Vol. 31, No. 3, 1993, pp. 426–433.

[5]Havener, G., and Stepanek, C., "Aero-Optical Testing Capabilities at AEDC," AIAA Paper 92-0760, Jan. 1992.
[6]Weinstein, L. M., "Large-Field High-Brightness Schlieren Systems," *AIAA Journal*, Vol. 31, No. 7, 1993, pp. 1250–1255.
[7]Gartenberg, E., Weinstein, L. M., and Lee, Jr., E. E., "Aerodynamic Investigation with Focusing Schlieren in a Cryogenic Wind Tunnel," *AIAA Journal*, Vol. 32, No. 6, 1994, pp. 1242–1249.
[8]Hughes, T. P., *Plasma and Laser Light*, Wiley, New York, 1975.
[9]Weinstein, L., Stacy, K., Vieira, J., Haering, Jr., E., and Bowers, A., "Imaging Supersonic Aircraft Shock Waves," *Journal of Flow Visualization and Image Processing*, Vol. 4, No. 3, 1997, pp. 189–199.
[10]Liepman, H. W., and Roshko, A., *Elements of Gas Dynamics*, Wiley, New York, 1967, pp. 157–162.
[11]Kafri, O., and Glat, I., *The Physics of Moire Metrology*, Wiley, New York, 1989.

R. P. Lucht
Associate Editor

Free Vibrations of Orthotropic Cylindrical Shell on Elastic Foundation

D. N. Paliwal* and Satyendra Singh†
Motilal Nehru Regional Engineering College, Allahabad 211 004, India

Nomenclature

C_1, C_2, C_3	= vibration amplitude constants in axial, tangential, and radial directions, respectively
E_1, E_2	= Young's moduli in x and ϕ directions, respectively
G	= shear modulus
G_{12}	= modulus of rigidity associated with principal material directions
$\bar{G}$	= nondimensional shear modulus, $G(1-\nu_{12}\nu_{21})/E_1 h$
h	= shell thickness
K	= foundation modulus
L	= length of cylindrical shell
m	= number of axial half-waves
n	= number of circumferential waves
R	= radius of middle surface of the shell
t	= time coordinate
U, V, W	= natural vibrational modes in the longitudinal, circumferential, and radial directions, respectively
u, v, w	= displacement components of the middle surface in axial, circumferential, and radial directions, respectively (w-positive inward)
α^2	= E_2/E_1
λ	= axial wave parameter, $\lambda^* R = m\pi R/L$
λ^*	= wave parameter, $m\pi/L$
$\bar{\mu}$	= nondimensional foundation parameter, $K R^2(1-\nu_{12}\nu_{21})/E_1 h$
ν_{12}, ν_{21}	= Poisson's ratios in x and ϕ directions, respectively
ρ	= mass density of structural material
Ω	= dimensionless frequency parameter
ω	= angular frequency

Introduction

CYLINDRICAL shells that have continuous and thorough contact with an elastic medium, solid or liquid, either on an outer or inner surface are considered as cylindrical shells on an elastic foundation. Such components and structures are often subjected to dynamic loads. Flow-induced vibrations in heat exchangers and pipelines, wave loading on submarines, vibrations of fuel-filled droptanks of fighter aircraft, underground and under-sea pipelines, and tunnels and semicircular roofs of underground aircraft hangers subject to seismic forces, nuclear explosions, and other blasts are some of the numerous examples.

Significant contributions have been made in the field of vibrations of cylindrical shells in general.[1–3] However, vibrations of isotropic shells on elastic foundations have been studied only recently.[4,5] Herein, the authors investigate the vibrations of an orthotropic cylindrical shell on an elastic foundation using membrane theory, inasmuch as the effect of the h/R ratio on the eigenfrequencies of thin cylinders is insignificant. Response of elastic media is represented by Winkler and Pasternak foundation models (see Ref. 6). Winkler represented an elastic foundation by a set of closely spaced, independent linear springs. Pasternak interconnected these springs through a shear layer made of incompressible vertical elements.

Analysis

Equations of motion for natural vibration of orthotropic circular cylindrical shell resting on a Pasternak foundation are as follows:

$$\frac{\partial^2 u}{\partial x^2} + \nu_{21}\frac{\partial}{\partial x}\left(\frac{\partial v}{R\partial\phi} - \frac{w}{R}\right) + \frac{G_{12}(1-\nu_{12}\nu_{21})}{E_1} \times \frac{\partial}{R\partial\phi}\left(\frac{\partial u}{R\partial\phi} + \frac{\partial v}{\partial x}\right) = \frac{\rho(1-\nu_{12}\nu_{21})}{E_1}\frac{\partial^2 u}{\partial t^2} \tag{1a}$$

$$\nu_{12}\alpha^2\frac{\partial^2 u}{R\partial\phi\partial x} + \alpha^2\frac{\partial}{R\partial\phi}\left(\frac{\partial v}{R\partial\phi} - \frac{w}{R}\right) + \frac{G_{12}(1-\nu_{12}\nu_{21})}{E_1} \times \frac{\partial}{\partial x}\left(\frac{\partial u}{R\partial\phi} + \frac{\partial v}{\partial x}\right) = \frac{\rho(1-\nu_{12}\nu_{21})}{E_1}\frac{\partial^2 v}{\partial t^2} \tag{1b}$$

$$\nu_{12}\alpha^2\frac{\partial u}{R\partial x} + \frac{\alpha^2}{R}\left(\frac{\partial v}{R\partial\phi} - \frac{w}{R}\right) = \frac{\rho(1-\nu_{12}\nu_{21})}{E_1}\frac{\partial^2 w}{\partial t^2} \times \frac{(1-\nu_{12}\nu_{21})}{E_1 h}(Kw - \bar{G}\nabla^2 w) \tag{1c}$$

Assuming that the cylindrical shell is simply supported at both ends, that is, $u(0)=0$, the general solution of Eq. (1) can be given by considering the boundary conditions in the form[7]

$$u = U(x)\cos n\phi\cos\omega t, \qquad v = V(x)\sin n\phi\cos\omega t$$
$$w = W(x)\cos n\phi\cos\omega t \tag{2}$$

where U, V, and W can be expressed as

$$U = C_1\cos\lambda^* x, \qquad V = C_2\sin\lambda^* x, \qquad W = C_3\sin\lambda^* x \tag{3}$$

By the substitution of solutions (2) and (3) into partial differential equations (1), the three algebraic equations are obtained as

$$\begin{aligned}
&\left(\Omega^2 - H_1\right)C_1 + n\lambda[\nu_{21} + (G_{12}/E_1)(1-\nu_{12}\nu_{21})]C_2 - \nu_{21}\lambda C_3 = 0\\
&n\lambda\left[(G_{12}/E_1)(1-\nu_{12}\nu_{21}) + \alpha^2\nu_{12}\right]C_1 + \left(\Omega^2 - H_2\right)C_2 + \alpha^2 n C_3 = 0\\
&-\nu_{12}\lambda\alpha^2 C_1 + \alpha^2 n C_2 + \left(\Omega^2 - H_3\right)C_3 = 0
\end{aligned} \tag{4}$$

For a nontrivial solution, the determinant of the coefficients of C_1, C_2, and C_3 must be zero. This yields the following bicubic equation for eigenfrequencies:

$$\bar{\Omega}^3 - \bar{\Omega}^2(H_1+H_2+H_3) + \bar{\Omega}\left[(H_1H_2 + H_2H_3 + H_3H_1) - \alpha^4 n^2 - \nu_{12}\nu_{21}\lambda^2\alpha^2 - n^2\lambda^2 P_1 P_2\right] - \left[H_1H_2H_3 - n^2\alpha^4 H_1 - n^2\lambda^2 P_1 P_2 H_3 - \nu_{12}\nu_{21}\lambda^2\alpha^2 H_2 - \nu_{12}n^2\lambda^2\alpha^4 P_2 - \nu_{12}n^2\lambda^2\alpha^2 P_1\right] = 0 \tag{5}$$

Received 25 November 1998; revision received 20 April 1999; accepted for publication 5 May 1999. Copyright © 1999 by the American Institute of Aeronautics and Astronautics, Inc. All rights reserved.

*Professor, Department of Applied Mechanics.
†Postgraduate Student, Department of Applied Mechanics.